Electrochemical Hydrogen Evolution on Pt-based Catalysts from A Theoretical Perspective

Ke-Xiang Zhang[1], Zhi-Pan Liu[1,2,3]*

[1]Collaborative Innovation Center of Chemistry for Energy Material, Shanghai Key Laboratory of Molecular Catalysis and Innovative Materials, Key Laboratory of Computational Physical Science, Department of Chemistry, Fudan University, Shanghai 200433, China

[2]Shanghai Qi Zhi Institution, Shanghai 200030, China

[3]Key Laboratory of Synthetic and Self-Assembly Chemistry for Organic Functional Molecules, Shanghai Institute of Organic Chemistry, Chinese Academy of Sciences, Shanghai 200032, China

Corresponding Author: *zpliu@fudan.edu.cn

Supplementary material

ABSTRACT: Hydrogen evolution reaction (HER) by splitting water is a key technology towards a clean energy society, where Pt-based catalysts were long known to have the highest activity under acidic electrochemical conditions but suffer from high cost and poor stability. Here we overview the current status of Pt-catalyzed HER from a theoretical perspective, focusing on the methodology development of electrochemistry simulation, catalytic mechanism, and catalyst stability. Recent developments in theoretical methods for studying electrochemistry are introduced, elaborating on how they describe the solid-liquid interface reactions under electrochemical potentials. The HER mechanism, the reaction kinetics, and the reaction sites on Pt are then summarized, which provides an atomic-level picture of Pt catalyst surface dynamics under reaction conditions. Finally, state-of-the-art experimental solutions to improve catalyst stability are also introduced, which illustrates the significance of fundamental understandings in new catalyst design.

1. INTRODUCTION

The past century has witnessed a surge in energy demand, predicted to approach 26 TW in 2040 around the world.[1] Despite many drawbacks of fossils, particularly their huge damage to climate, it is still the main energy source for economic and technical reasons, and the seek for a clean, efficient alternative becomes never been more urgent in recent years. Among the potential energy carriers, hydrogen molecule (H_2) is the one with outstanding advantages attracting much attention for its highest energy density and clean products while combusting.[2] On the other hand, to date H_2 is unfortunately mainly produced by the steam reforming process in the industry where the carbon source (CO) still comes from coal-based raw materials.[2, 3] It is therefore highly desirable to realize the massive production of H_2 using the clean route, such as the electrochemical water splitting, in which the half-cell hydrogen evolution reaction (HER, $H^+ + e^- \rightarrow 1/2\ H_2$) [2, 4] occurring on the cathode catalysts can generate hydrogen from water in a green way. [5, 6] The key challenge in the field is to find an active, abundant and stable cathode catalyst that is capable of massive H_2 production.[7] This perspective aims to review the current status of fundamental research on Pt-based HER catalysts.

Pt-based catalysts were long identified as the most efficient catalyst for HER under acidic conditions, achieving the highest exchange current density ~1 $mA{\cdot}cm^{-2}$ at room temperature, [8, 9] which has a diminished onset overpotential, excellent kinetics[10], and low Tafel slope[11]. Nevertheless, the high cost, poor earth-abundant, and low stability of the Pt catalysts strongly limit the wide applications in practice.[6, 12] For example, after 1,000 cycles of cyclic voltammetry (CV) between +0.4 V and -0.15 V vs. SHE in an acidic environment, the state-of-the-art commercial Pt/C catalyst has a loss of 19% of the current density at the overpotential of 0.05 V and the average particle size increase from 4.2 to 5.5 nm in the high-resolution transmission electron microscopy (HRTEM) images.[13] Furthermore, serious aggregation occurs as the potential becomes lower[14], suggesting that the high H coverage may induce high Pt mobility by weakening Pt-C support interaction. In addition, the direct dissolution of small Pt nanoparticles (<0.4 nm) could also trigger the Ostwald ripening for the growth of Pt nanoparticles and leads to the metal precipitate in the membrane of the proton exchange membrane water electrolyzer. [15-17] Therefore, it is a must not only to significantly reduce the expensive Pt content in cathode catalysts but also to improve markedly the long-term catalyst stability. To this goal, huge fundamental efforts have been devoted to understanding the HER reaction mechanism and the active site dynamics of Pt catalysts.

It is now clear that HER consists of three elementary reactions.[11] First, a proton in solution combines with an electron on the cathode to generate an adsorbed H* specie on

the metal surface, the so-called Volmer reaction ($H^+ + M + e^- \rightarrow M\text{-}H^*$). Then, H_2 can be generated via two routes. One is the Heyrovsky reaction where H* reacts with another H^+ in solution and e^- of the electrode to release H_2 ($M\text{-}H^* + H^+ + e^- \rightarrow M + H_2$). The other is the Tafel reaction where two surface H* atoms couple to become H_2 ($2M\text{-}H^* \rightarrow 2M + H_2$). According to the Butler-Volmer equation, the Tafel slopes should be 120 mV/dec (half-electron transfer), 40 mV/dec (one-and-half electron transfer), and 30 mV/dec (two-electron transfer) if the rate-determining step is the Volmer reaction, Heyrovsky reaction, and Tafel reaction, respectively.[18] Since the Tafel plot can be facilely obtained from the linear sweep voltammetry (LSV) curves in experiments, the HER on metals has been the model electrochemical reaction extensively studied in history to verify the electrochemical reaction theory. Interestingly, the measured Tafel slope for HER on Pt catalysts varies largely from experiment to experiment, which are often not at the characteristic values (120, 60, 40, 30 mV/dec), particularly on single crystal (111) surface where the measured Tafel slope is in a wide range of 37-300 mV/dec. [9, 19-22] Apparently, due to the too-fast kinetics of HER on Pt and the interference of aqueous solution and Pt surface structure variation, it is difficult to measure the accurate kinetics data of HER on Pt by experiment, particularly the reaction barrier and the pre-exponential factors of elementary steps are generally unknown.

On the other hand, the past two decades have seen the active development of theoretical methods for investigating electrochemical reactions. These methods generally rely on density functional theory (DFT) calculations and further consider the effects due to the solution and the external electrochemical potential at a certain level of approximations. [7] With these approximations, the delicate effects caused by the complex structural dynamics of the aqueous solution and the electrolyte under electrochemical potentials can be quantified properly, and thus the theory is capable to provide important insights into the HER kinetics, mechanism, and surface reconstructing under electrochemical potentials. [23-25] The relatively simple reaction network of HER on Pt surfaces is thus an ideal testing ground for accurate and low-cost electrochemistry simulations.

This perspective serves to summarize the recent theoretical and experimental advances in Pt-catalyzed HER. The paper is organized as follows. Section 2 describes the key methodology developed to model electrochemistry. This follows the theoretical efforts in the past decades to clarify the active site of HER on Pt-based catalysts in Section 3. In Section 4, we review the representative experimental means to improve the stability of Pt catalysts. At last, we provide our perspective on the future research of HER on Pt-catalysts.

2. Methodology for modeling electrochemistry

The electrochemical reactions occur at the solid-liquid interface where the external potential can be forced to keep constant with the help of a potentiostat device. The intimate coupling between the solid-liquid interface reaction and the electrochemical potential creates profound, complex, potential-dependent phenomena in electrochemical reaction systems. From a fundamental point of view, revealing the atomic structures of the interface under electrochemical conditions might be the first step towards understanding electrochemical reactions, which are however difficult to achieve not only in experiments but also in theory.

To properly account for electrochemical reactions, one, therefore, has to consider both the solid-liquid interface and the electrochemical potential accurately in one theoretical framework.[26] While quantum mechanics (QM) calculations based on DFT can be routinely utilized for solid surface calculations using a periodic slab model[27, 28], it is not straightforward to incorporate the solvation effect and the electrochemical potential effect within the current QM calculation framework. In principle, the brute-force molecular dynamics calculations based on QM calculations, that is, by adding a number of water and electrolyte molecules on top of solid surfaces, offers a possible solution for describing the dynamic nature of the solid-liquid interface, but the huge computational cost associated with QM calculations prevents such applications in a large-scale, not even mentioning the intrinsic difficulty of MD simulations in capturing reactions, the rare events. Furthermore, the constant potential condition applied in the experiment implies the grand canonical ensemble of the electron in the system, which can flow in and out at a constant chemical potential. The variable number of electrons in QM calculations thus raises another technique challenge, which could introduce huge instability of charge density in the self-consistent loop and thus slow greatly the energy convergence. In the following, we overview the current methodology to account for the electrochemical conditions.

2.1 Methods to describe solid-solution interface

The solvent not only controls the molecular adsorption/desorption equilibrium but also may directly take part in reactions at the interface, as most encountered in the proton-coupled electron transfer (PCET) reactions. For HER reaction on metals, both the Volmer and Heyrovsky steps involve the PCET and thus a reliable description of the electrolyte solution is essential for determining the activation energy and understanding the electrochemical reactions.

Before the advent of a more sophisticated solvation approach, a static ice-like hexagonal water bilayer model was adopted to account for the possible solvation effect, which is certainly much more convenient than long-time MD simulations. The ice-bilayer approximation is based on the surface science evidence, [29-31] which shows that the water hexagonal bilayer can form on Pt(111) surface below 150 K in ultrahigh vacuum, a stable configuration also confirmed by DFT calculations.[30] In such a bilayer, there are two alternating types of water (one close-packed layer of hexagonal ice), which

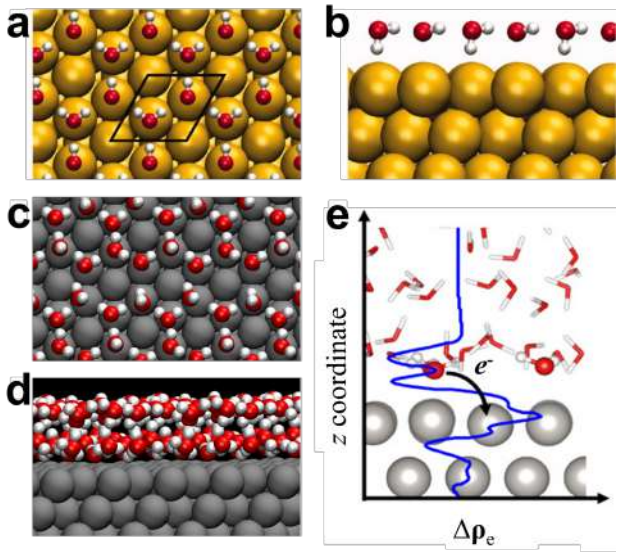

Figure 1. Typical model for the metal-water interfaces **(a, b)** H-down water bilayer. Reprinted from ref 33 with permission. Copyright 2012, John Wiley and Sons. **(c, d)** Snapshot of the disorder interface in AIMD after 11 ps. Adapted with permission from ref 37. Copyright 2012 Elsevier. **(e)** The interface of Pt(111)/H_2O at the potential of zero charge. The blue curve shows a charge redistribution along the z coordinate. Reproduced with permission from ref 38. Copyright 2020 with American Association for the Advancement of Science.

can interact with the metal surface either using the H or using the O. The former is known as the H-down bilayer and the latter is the H-up bilayer, the exact nature of the bilayer depending on the metal surfaces--- for Pt(111), the H-down water bilayer is thermodynamically more stable than the H-up water bilayer in moderate acidic HER condition.[32, 33] In the structure, one type of water molecule is parallel to the Pt(111) surface and bonds to the Pt atoms from the on-top sites, and the other type is perpendicular to the metal surface, as depicted in Figure 1(a, b). While the bilayer ice model is a rather crude approximation to water on Pt at ambient conditions, it does capture the essential physics of water-metal interaction. For example, the work function of Pt(111) drops markedly from ~5.9 eV in vacuum to ~4.9 eV in solution [34], which can be understood by the strong electrostatic screening of the H-down dipole. A single water bilayer even yields the capacitance of the double layer that is consistent with the experimental data [35] (the capacitance is determined by the curvature of the parabolic relation between the integral free energy of the double layer and the electrode potential). The dominance of the H-down configuration also provides a direct picture for how protons transfer from the solution to the surface and reacts with surface H in the Heyrovsky step (further discussed in Section 3). However, the direct MD simulations based on DFT at the room temperature by Gross and his coworkers [36, 37] demonstrate that the water layers on the Pt surface in fact deviate, to a large extent, from the ideal bilayer model with pronounced H-up water molecules. As can be seen in Figure 1(c, d), the snapshot of the H_2O/Pt(111) interface after 11 ps shows the disordered H_2O interface layer. A similar picture was then observed by Cheng and his coworkers in their DFT-MD simulations. [38, 39] Therein, a number of H-up waters are found to chemically adsorb on the metal and the charge moving from the water layer to the metal surface can induce the interface dipole potential (Figure 1(e)). It should be mentioned that these MD simulations were performed at the potential of zero charge (PZC), i.e. 0.2-0.3 V vs SHE[39]. Hence the H-down waters are expected to be dominant at the interface under HER conditions (0 V vs SHE).

For the investigation of interface chemical reactions, both the bilayer model using static calculations and the MD simulations of explicit multiple water layers meet great difficulties to get converged reaction energetics, since the results could be highly sensitive to the number of water molecules and their configurations in the model. In particular, the first principles MD simulations with a few picoseconds time-scale are generally far not enough for describing the the change of solvation shell during reactions. It thus asks for better solvation models to treat the solid-liquid interface.

In fact, implicit solvation models have long been utilized for molecular systems, generally known as the polarizable continuum model (PCM) based on the generalized Born model to describe the long-range electrostatic interaction between solution and solute. PCM models typically have several adjustable parameters, such as the solvation atomic radius and the atomic charge, which can be parametrized using the solvation data of molecules from experiments. However, the quantitative experimental data of solid surface solvation is generally not available, which delays the development of the analogous periodic implicit solvation models for the solid-liquid interface. From ~2008, several groups[19, 23, 26, 40-42] developed their own versions of the periodic implicit solvation model by solving the (modified) Poisson-Boltzmann (MPB) equation where the DFT charge density ρ and the dielectric distribution function $\varepsilon(r)$ are taken as the input following the work of Fattebert and Gygi.[43] The CM-MPB version, as shown in Eq. 1-3, developed by our group considers explicitly the counter charge (in electrolytes) to distribute in a manner of MPB equation(the right-hand second term in Eq. 1). Importantly, the approach can be utilized to obtain a reasonable electrochemical potential using Eq. 3 via a double-reference approach: first, referencing the Fermi level (Ψ_F) to the potential level of implicit solution (Ψ_{ref}) and then comparing to the absolute vacuum level SHE that is 4.44-4.85 V from experiments (typically the average value 4.6 V is used). [19, 23, 44, 45]

$$\nabla \cdot \left(\varepsilon(r)\nabla(\Psi)\right) = -4\pi\rho + 8\pi zec_b \frac{\sinh\left(\frac{ze\Psi}{kT}\right)}{1 - \nu + \nu\cosh\left(\frac{ze\Psi}{kT}\right)} \quad (1)$$

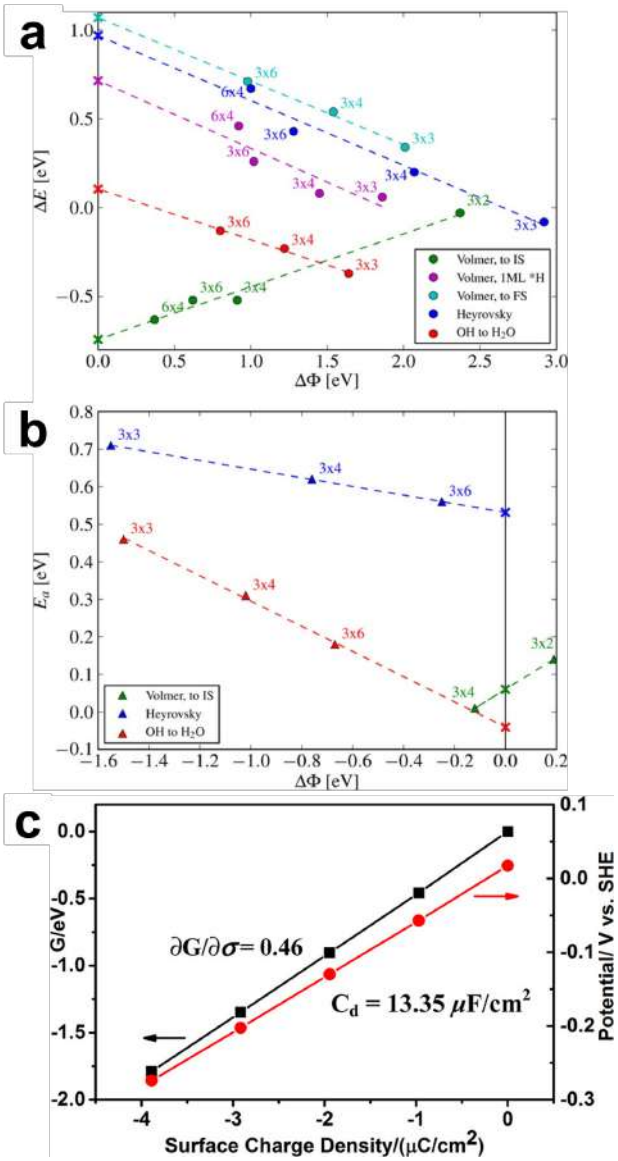

Figure 2. (a, b) Extrapolation scheme applied to the typical proton transfer reactions for both reaction energies and activation energies. Reprinted with permission from ref 56 (part of the data are taken from ref 35 and 55). Copyright 2015 American Chemical Society. **(c)** The fitting plot of the potential (U) and the free energy (G) versus the surface charge density σ changed in the CM-MPB scheme of a 1 ML H covered Pt(111) surface. Adapted with permission from ref 61. Copyright 2014 American Chemical Society.

$$\varepsilon\big(\rho(r)\big) = 1 + \frac{\varepsilon_\infty - 1}{2}\left[1 + \frac{1-(\rho(r)/\rho_0)^{2\beta}}{1+(\rho(r)/\rho_0)^{2\beta}}\right] \quad (2)$$

$$U_{\mathrm{cal}}^{q} = (\Psi_{\mathrm{ref}} - \Psi_{\mathrm{F}}) - 4.6 \quad (3)$$

In the equations, v is a parameter related to the electrolyte and satisfies $v=2a^3c_b$ (a is the effective ion size and c_b is the bulk concentration of electrolyte); the smooth dielectric function $\varepsilon(r)$ [43] is to provide a solvation environment of the continuum dielectric medium. The ρ_0 and β are the two key parameters where ρ_0 sets the threshold of electron density $\rho(r)$ and hence adjusts the cavity size, and β adjusts the smoothness of ε when changes from 1 to ε_∞ (78.36 for water in room temperature). The MPB equation can be solved facilely during the QM self-consistent loop as long as the $\varepsilon(r)$ is fixed. The implicit solvation model is known to fail when strong steric and directional polarization occurs (such as reactions with solvation proton) and thus typically a few extra explicit water molecules are required to account for the local polarization. [46] Nowadays many modern periodic DFT packages have the MPB solver (SIESTA, VASPsol, JDFTx, GPAW) and thus implicit solvation is routinely utilized in recent literature.

With the advent of machine learning (ML) potentials, explicit solvation via long-time MD simulation becomes feasible in recent years. For example, the free energy barrier of the solid-liquid interface reactions can be facilely determined by combining global neural network potential (G-NN) developed by our group with enhanced MD techniques (such as umbrella sampling). [47] [48] While such explicit solvation calculations can provide important insights into the effects due to the solvent and electrolytes, there are still severe limitations in the ML potential calculations. In particular, the current ML potentials lack electronic structure information, especially the charge density. It is thus not possible to read out readily the electrochemical potential from the calculation and also to polarize the interface under a preset potential. The electrochemical potential can be obtained by post-DFT calculations based on the MD trajectory from ML simulations.

2.2 Methods to control electrochemical potential

The electrochemical potential is the key variable controlled by the experiment to change the reaction rate. Compared to real experiments where the area of the interface is essentially infinite and a single charge transfer of reaction does not change the potential, theoretical simulations are limited by the small-sized supercells where the occurrence of reaction will inevitably lead to the change of electrochemical potential, no matter with or without the implicit/explicit solvation models. The thus-computed reaction kinetics are not accurate, where the initial (IS), transition (TS), and final states (FS) correspond to different electrochemical potentials. Therefore, to model electrochemical reactions at a given electrochemical potential on a given structure, a variable surface charge model to keep the potential constant as the structure changes needs to be developed.

The double-reference method proposed by Neurock and coworkers[49, 50] with explicit solvation and later utilized in the CM-MPB method as described in Eq. 1-3 is the common approach to determine the electrochemical potential. Basically, this method assumes the solution level is constant with respect to surface charging, where the counter-charge distribution will strongly affect the solution level in calculations. In periodic slab

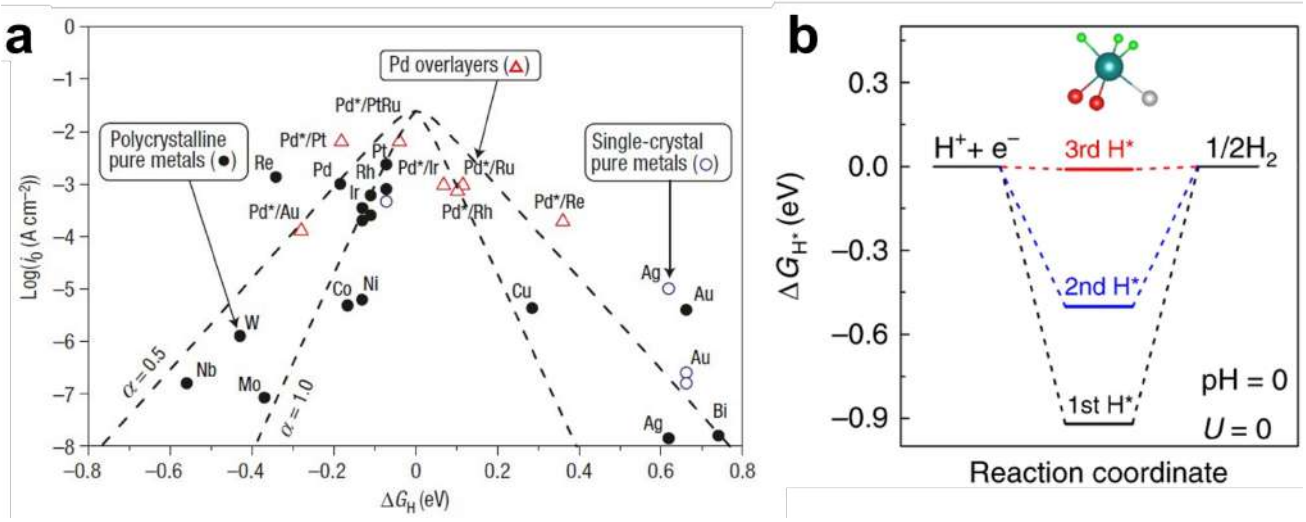

Figure 3. (a) HER volcano plot for a series of metal and metal overlayer. Reprinted from ref 78 with permission. Copyright 2006 Nature Publishing Group. **(b)** The free energy profile of 3 H atoms consecutively adsorbed on the Pt_1/OLC with the condition of pH 0 and equilibrium potential. Adapted with permission from ref 80. Copyright 2019 Springer Nature.

calculations, the counter-charges due to surface charging are automatically added for charge neutralization in a manner of homogenous background. The homogeneous background charge may however introduce wrong physics occasionally: unrealistic charges will move to the vacuum from the electrode[51] when the potential in the middle of the vacuum layer is lower than the work function of the metal; the added charge tends to delocalize on the electrode, making the charged defect calculations unlikely.[52, 53] Certainly, it is physically more appropriate to distribute the counter charge following the MPB equation, as implemented by our group using the CM-MPB method and recently in the solvated jellium (SJ) method[41, 54], where the counter charge is distributed in the implicit solution positions, the same as real anions/cations nearby the surface. The Debye lengths of the electrochemical double layer can be utilized to speed up the distribution of the countercharge with finite supercell sizes.[54]

Knowing the electrochemical potential of a given state, it further demands the alignment of potential between different reaction intermediate states, particularly the IS and the TS, to determine the reaction barrier of an electrochemical reactions. Early calculations using the ice-like bilayer model has shown a rather linear relationship between the energy changes and the potential changes, which validates the simple extrapolation methods either by using different-sized unit cells with the different number of excess hydrogen atoms, [35, 44, 55] as seen in Figure 2(a, b) or by using the charge-extrapolation method. [56, 57] Figure 2(a, b) presents respectively the reaction energy ΔE and activation energy E_a of some common charge transfer reactions against the potential change $\Delta\Phi$ in different cell sizes, and their extrapolation to the infinite cell size where $\Delta\Phi = 0$. A clear linear relation can be seen in Figure 2(a, b) except scatter in the situation of the Volmer reaction at 1 ML H*. Such scatter can be attributed to the slightly different H binding environment in different cell sizes.[56] To avoid the repeating calculations at different cell sizes in the cell-extrapolation scheme, the charge-extrapolation method was established by Chan et al. [56, 57], who assumed that (i) reaction energies between two states at a constant potential Φ_1 can be partitioned into a chemical part and an electrostatic part and (ii) The electrostatic part can be treated as basic capacitor energy, as shown in Eq. 4.

$$E_2(\Phi_1) - E_1(\Phi_1) = E_2(\Phi_2) - E_1(\Phi_1) + \frac{(q_2 - q_1)(\Phi_2 - \Phi_1)}{2} \quad (4)$$

In the equation, E, Φ, and q denote the DFT energy, DFT work function, and interfacial charge, respectively. It should be mentioned that the linearity between $\Delta E(\Phi) = E_2(\Phi) - E_1(\Phi)$ and Φ in Eq. 4, can be perturbed when the interfacial charge Δq changes nonlinearity that can be caused by many factors such as water structure variation between the IS and FS (or TS), the lateral interactions of adsorbates and adsorbates, and strong hybridization between atoms.[57, 58] According to the above equation, the energy change at constant potential (work function) Φ_1 can be calculated by the value of the energies, work functions, and interfacial charges of state 1 and state 2. The exact number of charges at the interface can be determined from DFT using charge-partition methods, such as Bader method [59, 60], or more generally, from the explicitly added charges in the CM-MPB framework. Both approaches can be further utilized to deduce the important kinetics quantity, the charge transfer coefficient α (q_2-q_1 between state 2 and state 1 at a constant potential).

In CM-MPB framework developed by our group, the added charge to the supercell accumulates on the surface (measured

by the surface charge density σ) and thus changes the work function. The charge transfer coefficient α can then be computed using Eq. 5, [61]

$$\alpha = \frac{SC_d\Delta\Phi}{\theta F} \quad (5)$$

where θ, F, S is the surface coverage, Faraday constant, and unit area of one surface atom. ΔΦ is the relative potential change from state 1 to state 2. The differential capacitance C_d can be obtained by a linear fitting between the charge density σ and the electrode potential U using Eq. (6).

$$C_d = \frac{\partial\sigma}{\partial U} \quad (6)$$

A typical plot of free energy (*G*) and potential (*U*) vs surface charge density is illustrated in Figure 2(c) Pt(111) covered with 1 ML H*. As shown, both C_d and *G* have a good linear relation to the surface charge density, which validates the accuracy of the charge-extrapolation method for metal surfaces and further leads to the classification of electrochemical reactions [61]. Recently Chan et al. [58, 62] developed a force-based method to acquire the electron transfer coefficient *α*. The charge difference between two states, such as IS and TS, can be converted to the first derivatives of atom-centered forces with respect to the applied field.

While the above conventional canonical DFT calculations with *a posteriori* grand canonical (GC) corrections are the most popular approach, direct GC calculations were also attempted in the past decades, where the chemical potential of the electrons instead of the number of electrons is fixed during DFT calculations. Melander and his coworkers[63] and Bonnet et al.[64] developed the GC-DFT approaches that can automatically adjust the surface charge to satisfy the constant-potential constraint. Similarly, the continuum description of the solvent and ions using the MPB equation can be applied to accurately control the potential. These methods, while being elegant in methodology, are still less utilized in the community, which could be due to the slower convergence of electronic structure.

3. HER activity of Pt catalyst

3.1 Experimental kinetics data

Despite it was long established that Pt catalysts perform the best in HER, there are still many debates on the reaction kinetics and its dependence on the catalyst structure. Early studies indicated that the HER activity appears to be rather insensitive to synthetic methods of Pt catalysts (the surface structure of Pt) [65-67]. However, with the development of single-crystal techniques [9, 68-72], more recent experiments tend to support that HER on Pt is in fact a highly structure-sensitive reaction. By measuring the electrochemical curves of Pt(111), Pt(100), and Pt(110), Markovic groups [9, 68, 69] and Conway groups [70-72] both found that the HER activity is affected by the choice of single-crystal surfaces. Nonetheless, their activity sequences are not exactly the same, where the Markovic group deduced the activity sequence (111) < (100) < (110), with the exchange current density (i_0) being 0.45, 0.60, and 0.98 mA/cm^2 at 303 K in 0.05 M H_2SO_4, respectively [9], while Conway group reports a different order (100) < (111) < (110). [70] Nevertheless, the fact that the ridged (110) surface is the most active is also consistent with the conclusion from the Hoshi group, who identified a linear relationship between the i_0 and the concentration of the step sites.[73-75] These experiments implied that a small fraction of the most active Pt(110) may entirely determine the HER activity, which thus reconciles with the structure insensitivity observed in early experiments. These active sites may further be created dynamically by surface reconstruction during electrochemical HER cycles.

According to the measured Tafel slope, the Markovic group deduced the apparent charge transfer coefficients, 2 for (110) and 1 for (111). As for the (100), there are two distinct regions with different charge transfer coefficients, 1.5 for low overpotential and 0.5 for high overpotential. In fact, the measured Tafel slope for (111) surface varies largely and corresponds to the apparent charge transfer coefficients from ~1.6 to ~0.2.[9, 19-22] The Arrhenius plots between the logarithm of i_0 and 1/T from the Markovic group give the apparent activation energy being 0.19, 0.12, and 0.10 eV for (111), (100), and (110), respectively. [9] However, in a recent experiment by He et al.,[20] the apparent activation energy value of Pt(111) is in the range of 0.5 and 0.7 eV, which varies with the potential and is much larger than the result of Markovic. The large differences in the kinetics data between experiments suggest the intrinsic difficulty in measuring accurately the fast HER kinetics, where the entropy effects in proton transfer could play important roles. [20, 26, 52]

For Pt nanoparticles, the HER activity appears to be even more complex, being sensitive to the size of the particle.[76, 77] Klein et al[76] prepared a series of Pt nanoparticles with various scales from 25 atoms to 110 atoms and found that the HER activity has a volcano-like shape against the particle size. When the number of atoms is approximately 38, the HER activity reaches its maximum with the mass-specific current density being ~5.27 A mg_{Pt}^{-1}, while it is ~0.14 A mg_{Pt}^{-1} and ~0.11 A mg_{Pt}^{-1} for Pt_{25} and Pt_{110}, respectively. By monitoring the HER kinetics of Pt nanoparticles increasing the size from 1 atom to ~8 nm, Zhou et al.[77] observed a limiting plateau of non-normalized HER kinetics at ~4 nm, which supports that HER occurs on metallic Pt and the defected sites at corners or after surface reconstruction are the key active sites.

The surface dependence and the size dependence of HER kinetics on Pt pose challenges for theoreticians to understand the structure-activity relationship of HER on Pt. The key questions are *(i) why Pt(110), or more generally, the defected sites have the higher HER activity*; *(ii) which elementary reaction, Volmer, Tafel, or Heyrovski step, is the rate-determining step of HER.*

3.2 Mechanism and kinetics from theory

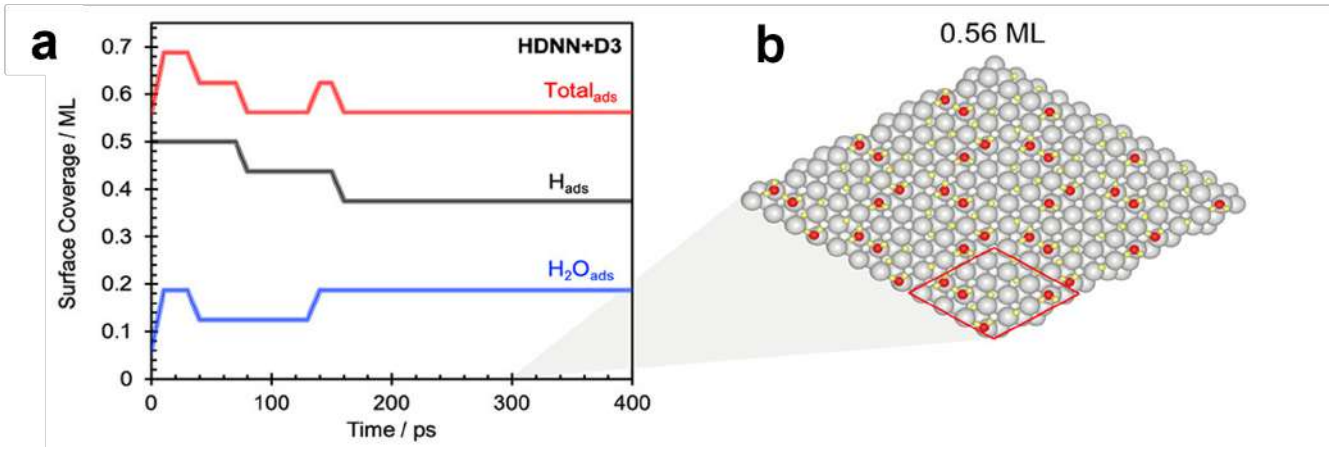

Figure 4. (a) Surface coverage evolution of H_{ads} and H_2O_{ads} during a 400 ps high-dimensional neural network potential (HDNN)-MD with D3 correction. **(b)** Snapshots after 300 ps with a total H coverage being 0.56 ML. Reprinted with permission from ref 47. Copyright 2021 American Chemical Society.

The most popular explanation of why Pt is the most active is the thermodynamics arguments proposed by the Nørskov group.[8, 78] They introduced the adsorption free energy of the hydrogen (ΔG_H) at the equilibrium potential as the descriptor to evaluate the catalytic performance of catalysts for HER. This is because the free energy of an adsorbed H atom can be referenced to half of a hydrogen molecule by DFT and further related to a single proton together with a single electron at a certain electrochemical potential by using a computational hydrogen electrode (CHE) approach. The HER activity of catalysts (represented by the exchange current density i_0) from the experiment against the computed ΔG_H does show a volcano-like shape, as illustrated in Figure 3(a). As can be seen, Pt locates at the peak of the volcano with its ΔG_H approaching 0. [78] The closer ΔG_H approaches 0, the more efficient the catalyst is, which is a thermodynamics consequence from the Sabatier principle and the Brønsted-Evans-Polanyi(BEP) relation.[79] The too large ΔG_H value (poor H adsorption) hinders the electrochemical adsorption of the proton, while the too low ΔG_H goes against the release of hydrogen. A typical application of the CHE approach can be seen in Figure 3(b) as an experimental example. In this example, the single Pt atom anchored on an onion-like carbon (OLC) nanosphere was synthesized, which has the ability to adsorb 3 H atoms and the adsorption free energy of the third H atom is -0.01 eV. [80] This explains why the catalyst has a high HER activity.

While the CHE approach provides a convenient and quick way to compare the catalytic activity between materials in a wide range without searching for the detailed reaction pathway, one must recognize that the thermodynamics approach is a crude approximation by neglecting a number of key issues to reaction kinetics, such as the surface H coverage effects, the solution effect, and the surface structure reconstruction. Indeed, none of the questions raised above, Pt(110) being more active and the rate-determining step of HER, can be answered by the ΔG_H thermodynamics. These questions are certainly the key to searching for the best catalyst at the peak of the volcano plot.

As for the kinetics, the activation energy of the Tafel step (H*+H*) on Pt(111) surface was most computed in literature, which yields the value from 0.40 to 1.00 eV. [19, 35, 41, 47, 52, 81] The computational models (e.g. H coverage, the H_2O numbers) and the computational methods, e.g. the choice of exchange-correlation functional (PBE or RPBE) and the solvation approaches appear to strongly affect the computed kinetics data. No consensus is achieved for the rate-determining step, although the Volmer-Tafel mechanism dominating the HER on the (111) surface appears to be more accepted. By the combination of the cell-extrapolation, explicit water bilayer model, and DFT-nudged elastic band (NEB) methods, Skulason et al. [35] found that on Pt(111) surface, the free energy barriers around the equilibrium potential are 0.69, 0.85, and 1.40 eV with RPBE functional for Volmer, Tafel, and Heyrovsky reaction respectively, with the H coverage being ~1 ML from the thermodynamic analysis. Their results suggest that the Volmer-Tafel pathway is the main mechanism of Pt(111) and the Tafel reaction is the rate-determining step. At 303 K, the exchange rate calculated by the Tafel barrier of 0.85 eV is 5.1×10^{-5} A/cm^2, which approaches the experimental value of 4.5×10^{-5} A/cm^2 by Markovic. [9] By using the DFT-NEB method, Marcus theory, and microkinetic simulation, Lindgren [41] found the free energy barriers are ~0.27 eV for the Volmer reaction and ~0.40 eV for the Tafel reaction at 0 V vs SHE in the SJ method. Their microkinetic simulation suggested that the coupling of two adjacent overpotential-deposited H on top sites leads to a Tafel slope of 30 mV/dec. On the other hand, Fang et al. [19] applied the CM-MPB model to describe the interface and Constrained-Bryoden minimization (CBD) Scheme to determine the TS, which found that the free energy barrier of Volmer reaction at 0 V vs. SHE on Pt(111) is lower

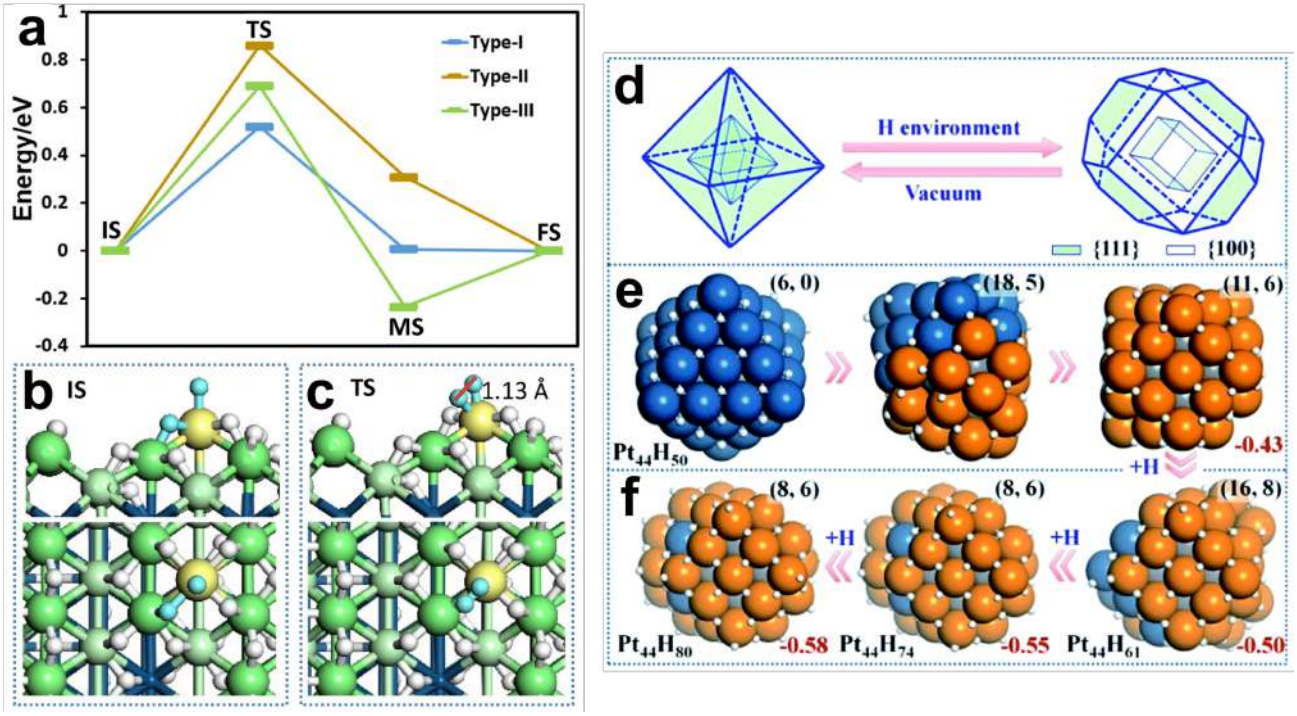

Figure 5. Reconstruction of Pt surfaces in H-abundant environment. **(a)** Free energy profile of Tafel reaction on three different types of Pt(110) surfaces at equilibrium potential. The IS and TS on Type-I surface are shown in **(b)** and **(c)** Reprinted with permission from ref 23. Copyright 2021 American Chemical Society. **(d-f)** Structure evolution of Pt_{44} clusters with increasing H adatoms. **(d)** A polyhedron demonstration of the evolution of Pt_{44} nanoparticles from octahedron to tetradecahedron; **(e)** the typical structures of $Pt_{44}H_{50}$ showing the reconstruction from (111) to (100); **(f)** the global minimum structures of $Pt_{44}H_{61}$, $Pt_{44}H_{74}$ and $Pt_{44}H_{80}$. Adapted with permission from ref 24. Copyright 2014 Royal Society of Chemistry.

than 0.2 eV, while the values of Heyrovsky reaction and Tafel reaction are both ~0.92 eV with the H coverage of ~1 ML at the PBE level. The Tafel slope is deduced to be 83 mV/dec for (111) from microkinetics, suggesting a mixed mechanism of Volmer-Tafel and Volmer-Heyrovsky on (111) surface. By contrast, Tang et al. 81 used the charge-extrapolation method to determine the HER kinetic barriers with explicit water. The barriers of Volmer, Tafel, and Heyrovsky steps at Pt(111), with H coverage being around the 1 ML, are 0.61 eV, 0.77-0.83 eV, and 0.62-0.74 eV in BEEF-vdW functional, respectively. Their calculated Tafel slopes deduced from the mean-field microkinetic simulation are ~120 mV/dec for Pt(111), suggesting the Volmer-Heyrovsky is the controlling mechanism.

Beyond the static TS search approaches using DFT calculations, enhanced MD methods have also been utilized to evaluate the barrier of elementary steps. Using a model of 180 Pt atoms and 160 explicit water molecules, the thermodynamic integration simulation at the equilibrium electrode potential by Kronberg and Laasonen52 yields the free energy barriers of 0.69 eV (1 ML H coverage) and 0.67 eV (0.66 ML H coverage) for the Volmer reaction and 0.53 eV (1 ML H coverage) and 0.80 eV (0.66 ML H coverage) for the Tafel reaction at Pt(111), respectively. After the charge-extrapolation method to correct the potential dependence of the barrier of the Volmer reaction (hydrogen adsorption is endergonic), the rate-determining step is still the Tafel step, although the Heyrovsky reaction is not considered in their work. Recently, Rice et al. 47 employed the global neural network (G-NN) potential to speed up the umbrella sampling MD simulations, which extends greatly the simulation time to ~400 ps. Their model is a 202-atom unit cell with 44 H_2O molecules and 2 solvated Cl atoms. Importantly, at equilibrium, the total equilibrium coverage of H_{ads} and H_2O_{ads} is found to be 0.56 ML with Vdw (D3) correction, as depicted in Figure 4(a), which is different from the commonly utilized ~1 ML from thermodynamics analysis. As can be seen in Figure 4(b), in the structure at the equilibrium, the H_{ads} atoms prefer the 3-fold fcc-hollow sites while H_2O_{ads} molecules tend to locate on the top site. The total coverage is in good accordance with the experimental result of 0.66 ML from Markovic. 9 They further showed that the Tafel barrier is 0.83 eV while the Heyrovsky barrier varies from 0.89 eV at 0.56 ML to 0.82 eV at 0.33 ML. They concluded that the Volmer-Tafel mechanism is preferred at high H coverage and the Volmer-Heyrovsky channel opens at low H coverages, suggesting a mixed mechanism on Pt(111).

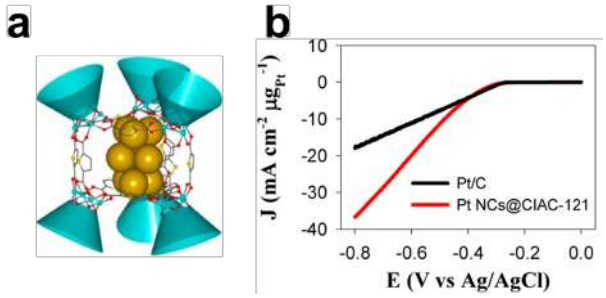

Figure 6. (a) The structure of Pt NCs@CIAC-121. **(b)** Linear sweep curves of the Pt NCs@CIAC-121 and Pt/C for HER in 0.5 M H_2SO_4 at a scan rate of 50 mV/s. Reprinted with permission from ref 98. Copyright 2016 American Chemical Society.

As for the most active Pt(110), the unreconstructed (1x1) surface is found to have a barrier of ~0.75 eV for the Tafel step 26, 35. Recently, by simulating cyclic voltammetry response, Fang et al.23 suggested that the high activity of Pt(110) may arise from the surface reconstruction, where single Pt atoms migrate away from the ridge forming a special five-coordinated Pt ([PtH_5], Pt_{5c}) sites locating at the trough. The stochastic surface walking–neural network (SSW-NN) invented by our group was utilized to explore the probable reconstruction pathways for Pt(110) facet at different electrochemical potentials and identified several types of surface sites (Type-I, II, and III in Figure 5(a)). Among, the Pt_{5c} sites (Type-I site in Figure 5(a-c)) is the most active, yielding the free energy barrier of the Tafel reaction of 0.52 eV at the equilibrium potential. The barrier is not only much lower than the HER free energy barrier ~0.9 eV on Pt(111) and Pt(100) in their previous work but also lower than that on the bulk-truncated Pt(110) ones ~0.75 eV. 26, 35

The surface reconstruction of Pt nanoparticles was in fact observed earlier by SSW-DFT simulations. Wei et al.24 investigated the structure evolution of a Pt_{44} nanoparticle starting from the high-symmetry octahedron $Pt_{44}H_{50}$ (at 1 ML H coverage) and the results are shown in Figure 5(d-f). Under the electrochemical potential, more H can adsorb on the nanoparticle surface, which induces the surface reconstruction toward exposing more (100) facets. This is caused by the higher H adsorption capacity of (100) than (111). In addition, the Tafel mechanism via H-H coupling at the apex site, the Pt_{5c} sites, of $Pt_{44}H_{80}$ is found to have the lowest free energy barrier in the range of 0.47-0.71 eV among all the sites considered, which validates that the high HER activity of Pt should come from the defected sites, which can be created by surface reconstruction. It might be mentioned that Tan et al.82 also studied the configuration evolution of a Pt_{55} nanoparticle with adsorbed H* atoms by using Monte Carlo (MC) simulations. However, because they did not consider the surface reconstruction and thus the Pt_{5c} site is not present in their model, the most active site is found to be at the (100) terrace site with a barrier of 0.62 eV.

4. Metal-support interaction and strategies to improve Pt catalyst stability

Since H adsorption induces significant reconstruction of Pt surfaces and nanoparticles that occurs under HER conditions, a strong metal-support interaction is highly desirable to prevent the detachment of metal nanoparticles from the support. On the other hand, with the massive production of H_2, the type of support must have a good enough electronic conduction ability in the first place, which led to the graphite-based material as the practical choice. In fact, various other supports such as $MoS_2$83, WC84, Nafion85, and nanopore stainless steel86 have been tested as the support in the literature, but the decay of the activity in the long-term remains obvious.

The weak interaction between Pt and graphite may be the reason for the low durability of the Pt/C catalyst. By using DFT calculations, Esposito et al. 87 showed that the binding energy of monolayer Pt-graphite C(0001) is ~24% lower than that of Pt-Pt in DFT calculations, which indicates that the agglomeration of Pt is inevitable in defect-free graphite. In addition, the electron transfer between Pt and graphite-based support is quite low. Nakada and Ishii applied the Bader analysis to research the charge transfer between single atoms of different elements and graphene monolayer. Among the first 83 elements on the Periodic Table, Pt and Au are the only two metallic elements where the direction of charge transfer is from the graphene to the single metal atoms and the transferred electrons are almost zero for Pt. 88 The low charge transfers (less than 0.1 e^- per Pt atom) were also reported for Pt clusters with around 40 atoms on the defect-free graphene, while the direction of charge transfer is in debate. 89-92 Apparently, due to the low interaction between Pt and pristine graphite-based materials, the key to improving the stability of Pt/C catalyst is to introduce defects to the carbon materials. Combined HRTEM with DFT calculations, Poidevin et al. 93 showed that Pt clusters do have a strong interaction with the zigzag edge of a basal plane of carbon black --- a Pt_{37} nanocluster is found to move to a zig-zag edge of the $C_{126}H_{30}$ support in DFT optimization with the interaction energy of -6.54 eV and 0.89 electron transfer from support to Pt. In the meantime, two planar carbon atoms with sp^2 hybridization convert to ones with sp^3 hybridization. The distortion of both the cluster and support is observed in the HRTEM images.

Recent experiments have made encouraging progress in stabilizing Pt nanoparticles or single atoms via modified carbon materials 13, 80, 94-97. For example, Cheng et al. 13 used the atomic layer deposition (ALD) method to anchor the Pt single atoms and small clusters on the nitrogen-doped graphene nanosheets (NGNs). The sample (ALD50Pt/NGNs) treated by 50 ALD cycles in 523 K has an overpotential (η_{10}) of ~50 mV when the current density is 10 mA cm^{-2} and shows only a 4% loss of the current density at 0.05 V overpotential after 1000 CV cycles from +0.4 to -0.15 V versus SHE with 100 mV/s. Their DFT calculations show that the single Pt atom has an adsorption

energy of -5.171 eV on the NGNs, and the normalized X-ray absorption near edge structure (XANES) indicate that ALD50Pt/NGNs have more unoccupied Pt 5d density of states than the commercial Pt/C catalyst. The high activity and durability of subnano Pt particles (less than 10 Pt atoms) on single-walled carbon nanotubes (SWNT) were reported by Tavakkoli et al.94, in which η_{10} is 27 mV and maintains largely after 5000 stability cycles. The adsorption energy of an isolated Pt on the SWNT axial site is -2.38 eV from their DFT results, which is 0.4-0.5 eV more exothermic than that on graphene. Yin et al.96 synthesized a single Pt atom catalyst on graphdiyne supports, featuring the four-coordinated C_2-Pt-Cl_2 species (Pt-GDY2). From their XPS and XANES analyses, the valence state of Pt in Pt-GDY2 is between 0 to +2. DFT calculations on the Pt-GDY2 indicate the H adsorption free energy is close to zero (+0.092 eV), supporting the good HER activity of the single-atom catalyst with η_{10} being ~50 mV. The stability of Pt-GYD2 is also high, since the LSV curve after 1000 cycles resembles the initial one, and the current density is almost constant at -95 mV for 10,000 s.

In addition, cage materials were also found to improve the stability of Pt-based HER catalysts via the confinement effect. Wang et al.98 used the trigonal prismatic coordination cages $\{Ni_{24}(TC4A\text{-}SO_2)_6(TDC)_{12}(H_2O)_6\}$ (CIAC-121) to imprison Pt clusters. The structure of as-synthesized Pt NCs@CIAC-121 is illustrated in Figure 6(a). The TEM images and mass spectra indicate that the Pt nanocluster is successfully encapsulated in the CIAC-121 without changing the morphology of CIAC-121 dramatically. Such Pt NPs@CIAC-121 catalyst has a η_{10} of 26 mV in 0.5 M H_2SO_4, as shown in Figure 6(b), and the activity remains over 75% after 5000 cycles of CV from 0 to -0.6 V.

5. Perspective

This work overviews the current status of Pt-catalyzed HER from a theoretical point of view. We emphasize the importance of the theoretical methodology developments in the past decades, which bypass the CHE thermodynamics analysis and lead to a better description of the solid-liquid interface and more accurate control of the electrochemical potential. Theory can now provide potential-dependent reaction profiles for solid-liquid electrochemical reactions, which was not possible 20 years ago. We note that newly emerged methods have already shown great potentials for the future research. In particular, the machine-learning potential techniques facilitate the global reaction search and long-time MD simulations. They are thus able to provide deep insights into the proton-coupled electron transfer reactions that are unique to solid-liquid interface reactions. On the other hand, the grand-canonical constant-potential simulations based on the first principles calculation framework appear to be a general and simple framework that facilitates to reach a consensus on the kinetics data in the community. While the direct combination of the above two, machine-learning potential and constant-potential simulations, is still a huge challenge, the CM-MPB model with constant-potential calculations is a practical solution.

By joint experiments and theoretical efforts, stepped Pt surfaces are recognized as the active site of Pt-based catalysts. The five-coordinated Pt atom ($[PtH_5]$ under reaction conditions) being present both at the Pt(110) trough and the apex site of Pt nanoparticles is the key surface site responsible for the activity, where the Tafel step for the H-H coupling between the top-H and the bridging H has a barrier as low as 0.5 eV. The less active but dominant Pt(111) surfaces remain controversial on the reaction mechanism, but a mixed Volmer-Tafel and Volmer-Heyrovsky mechanism is likely to reconcile existing literature, where the switch between pathways depends on the potential and the H coverages.

It is generally accepted on the high H coverage of Pt surfaces and nanoparticles under reaction conditions and the H-induced Pt surface reconstruction revealed from theoretical simulations complements the experimental data from CV curves. The low-stability Pt catalysts can now be understood by the H-induced detachment of Pt nanoparticles from support. Among various experimental means to improve Pt-support interaction, the anchoring of single Pt atoms and the confinement of subnano Pt particles are the most promising frontiers demonstrated in recent experimental advances. On the other hand, more and more research focused on non-Pt catalysts aiming to reduce the cost of HER catalysts. The semiconducting 2-dimensional MoS_2 99-103, Ni-based catalysts104-107, and Co-based catalysts108-110 were reported, althoughtheir activities are generally less satisfactory compared to Pt.6 Nevertheless, it is encouraging that the advance in electrochemical simulations also benefits greatly these non-Pt HER studies and promotes new catalyst design therein.

NOTES

The authors declare no competing financial interests.

ACKNOWLEDGMENT

This work was supported by the National Key Research and Development Program of China (2018YFA0208600), National Science Foundation of China (12188101, 22033003, 91945301, 91745201, 92145302, 22122301, 92061112) and the Tencent Foundation for XPLORER PRIZE.

REFERENCE

[1]Z. W. Seh, J. Kibsgaard, C. F. Dickens, I. Chorkendorff, J. K. Norskov and T. F. Jaramillo, Science **355** (6321), eaad4998 (2017).
[2]C. G. Morales-Guio, L. A. Stern and X. Hu, Chem. Soc. Rev. **43** (18), 6555 (2014).
[3]J. Hou, Y. Wu, B. Zhang, S. Cao, Z. Li and L. Sun, Adv. Funct. Mater. **29** (20), 1808367 (2019).
[4]R. d. Levie, J. Electroanal. Chem. **476**, 92 (1999).
[5]Q. Gao, W. Zhang, Z. Shi, L. Yang and Y. Tang, Adv. Mater. **31** (2), 1802880 (2019).

[6]X. Li, X. Hao, A. Abudula and G. Guan, J. Mater. Chem. A **4** (31), 11973 (2016).
[7]Q. Li, Y. Ouyang, S. Lu, X. Bai, Y. Zhang, L. Shi, C. Ling and J. Wang, Chem. Commun. **56** (69), 9937 (2020).
[8]J. K. Nørskov, T. Bligaard, A. Logadottir, J. R. Kitchin, J. G. Chen, S. Pandelov and U. Stimming, J. Electrochem. Soc. **152** (3), J23 (2005).
[9]N. M. Markovic, B. N. Grgur and P. N. Ross, J. Phys. Chem. B **101**, 5405 (1997).
[10]J. Wang, F. Xu, H. Jin, Y. Chen and Y. Wang, Adv. Mater. **29** (14), 1605838 (2017).
[11]J. Zhu, L. Hu, P. Zhao, L. Y. S. Lee and K. Y. Wong, Chem. Rev. **120** (2), 851 (2020).
[12]H. Jin, C. Guo, X. Liu, J. Liu, A. Vasileff, Y. Jiao, Y. Zheng and S. Z. Qiao, Chem. Rev. **118** (13), 6337 (2018).
[13]N. Cheng, S. Stambula, D. Wang, M. N. Banis, J. Liu, A. Riese, B. Xiao, R. Li, T. K. Sham, L. M. Liu, G. A. Botton and X. Sun, Nat. Commun. **7**, 13638 (2016).
[14]P. Paciok, M. Schalenbach, M. Carmo and D. Stolten, J. Power Sources **365**, 53 (2017).
[15]L. Tang, X. Li, R. C. Cammarata, C. Friesen and K. Sieradzki, J. Am. Chem. Soc. **132** (33), 11722 (2010).
[16]A. V. Virkar and Y. Zhou, J. Electrochem. Soc. **154** (6), B540 (2007).
[17]H. Yu, L. Bonville, J. Jankovic and R. Maric, Appl. Catal. B: Environ. **260**, 118194 (2020).
[18]R. G. Compton and C. E. Banks, *Understanding Voltammetry*. (World Scientific Publishing Europe Ltd., 2018).
[19]Y.-H. Fang, G.-F. Wei and Z.-P. Liu, J. Phys. Chem. C **117** (15), 7669 (2013).
[20]Z. D. He, J. Wei, Y. X. Chen, E. Santos and W. Schmickler, Electrochim. Acta **255**, 391 (2017).
[21]I. Ledezma-Yanez, W. D. Z. Wallace, P. Sebastian-Pascual, V. Climent, J. M. Feliu and M. T. M. Koper, Nat. Energy **2** (4), 17031 (2017).
[22]H. Ooka, M. E. Wintzer and R. Nakamura, ACS Catal. **11** (10), 6298 (2021).
[23]Y.-H. Fang, D.-d. Song, H.-x. Li and Z.-P. Liu, J. Phys. Chem. C **125** (20), 10955 (2021).
[24]G. F. Wei and Z. P. Liu, Chem. Sci. **6** (2), 1485 (2015).
[25]Y. Zheng, Y. Jiao, A. Vasileff and S. Z. Qiao, Angew. Chem. Int. Ed. Engl. **57** (26), 7568 (2018).
[26]M. Van den Bossche, E. Skúlason, C. Rose-Petruck and H. Jónsson, J. Phys. Chem. C **123** (7), 4116 (2019).
[27]M. C. Payne, M. P. Teter, D. C. Allan, T. A. Arias and J. D. Joannopoulos, Rev. Mod. Phys. **64** (4), 1045 (1992).
[28]Y. F. Shi, P. L. Kang, C. Shang and Z. P. Liu, J. Am. Chem. Soc. **144** (29), 13401 (2022).
[29]A. Verdaguer, G. M. Sacha, H. Bluhm and M. Salmeron, Chem. Rev. **106** (4), 1478 (2006).
[30]H. Ogasawara, B. Brena, D. Nordlund, M. Nyberg, A. Pelmenschikov, L. G. Pettersson and A. Nilsson, Phys. Rev. Lett. **89** (27), 276102 (2002).
[31]M. Nakamura, Y. Shingaya and M. Ito, Chem. Phys. Lett. **309**, 123 (1999).
[32]A. Michaelides, Appl. Phys. A **85** (4), 415 (2006).
[33]K. Tonigold and A. Gross, J. Comput. Chem. **33** (6), 695 (2012).
[34]Y. H. Fang, G. F. Wei and Z. P. Liu, Catal. Today **202**, 98 (2013).
[35]E. Skulason, V. Tripkovic, M. E. Bjorketun, S. Gudmundsdottir, G. Karlberg, J. Rossmeisl, T. Bligaard, H. Jonsson and J. K. Norskov, J. Phys. Chem. C **114** (50), 22374 (2010).
[36]S. Schnur and A. Gross, New J. Phys. **11**, 125003 (2009).
[37]T. Roman and A. Gross, Catal. Today **202**, 183 (2013).
[38]J. B. Le, Q. Y. Fan, J. Q. Li and J. Cheng, Sci. Adv. **6** (41), eabb1219 (2020).
[39]J. B. Le, M. Iannuzzi, A. Cuesta and J. Cheng, Phys. Rev. Lett. **119** (1), 016801 (2017).
[40]R. Jinnouchi and A. B. Anderson, Phys. Rev. B **77** (24), 245417 (2008).
[41]P. Lindgren, G. Kastlunger and A. A. Peterson, ACS Catal. **10** (1), 121 (2020).
[42]K. Mathew, R. Sundararaman, K. Letchworth-Weaver, T. A. Arias and R. G. Hennig, J. Chem. Phys. **140** (8), 084106 (2014).
[43]J. L. Fattebert and F. Gygi, J. Comput. Chem. **23** (6), 662 (2002).
[44]Y. H. Fang and Z. P. Liu, J. Am. Chem. Soc. **132** (51), 18214 (2010).
[45]Y.-H. Fang and Z.-P. Liu, ACS Catal. **4** (12), 4364 (2014).
[46]A. Gross and S. Sakong, Chem. Rev. **122**, 10746 (2022).
[47]P. S. Rice, Z. P. Liu and P. Hu, J. Phys. Chem. Lett. **12** (43), 10637 (2021).
[48]L. H. Luo, S. D. Huang, C. Shang and Z. P. Liu, ACS Catal. **12** (10), 6265 (2022).
[49]J. S. Filhol and M. Neurock, Angew. Chem. Int. Ed. Engl. **45** (3), 402 (2006).
[50]C. D. Taylor, S. A. Wasileski, J. S. Filhol and M. Neurock, Phys. Rev. B **73** (16), 165402 (2006).
[51]A. Gross and S. Schnur, in *Catalysis in Electrochemistry*, edited by E. Santos and S. Wolfgang (John Wiley & Sons, Inc., 2011), pp. 165-192.
[52]R. Kronberg and K. Laasonen, ACS Catal. **11** (13), 8062 (2021).
[53]H. P. Komsa and A. Pasquarello, Phys. Rev. Lett. **110** (9), 095505 (2013).
[54]G. Kastlunger, P. Lindgren and A. A. Peterson, J. Phys. Chem. C **122** (24), 12771 (2018).
[55]J. Rossmeisl, E. Skulason, M. E. Bjorketun, V. Tripkovic and J. K. Norskov, Chem. Phys. Lett. **466**, 68 (2008).
[56]K. Chan and J. K. Norskov, J. Phys. Chem. Lett. **6** (14), 2663 (2015).
[57]K. Chan and J. K. Norskov, J. Phys. Chem. Lett. **7** (9), 1686 (2016).
[58]S. Vijay, G. Kastlunger, J. A. Gauthier, A. Patel and K. Chan, J. Phys. Chem. Lett. **13** (25), 5719 (2022).
[59]R. F. W. Bader, Chem. Rev. **91** (5), 893 (1991).
[60]G. Henkelman, A. Arnaldsson and H. Jonsson, Comput. Mater. Sci **36** (3), 354 (2006).
[61]Y. H. Fang, G. F. Wei and Z. P. Liu, J. Phys. Chem. C **118** (7), 3629 (2014).
[62]A. M. Patel, S. Vijay, G. Kastlunger, J. K. Norskov and K. R. Chan, J. Phys. Chem. Lett. **12** (21), 5193 (2021).
[63]M. M. Melander, M. J. Kuisma, T. E. K. Christensen and K. Honkala, J. Chem. Phys. **150** (4), 041706 (2019).
[64]N. Bonnet, T. Morishita, O. Sugino and M. Otani, Phys. Rev. Lett. **109** (26), 266101 (2012).
[65]K. Seto, A. Iannelli, B. Love and J. Lipkowski, J. Electroanal. Chem. **226**, 351 (1987).
[66]S. Schuldiner, M. Rosen and D. R. Flinn, J. Electrochem. Soc. **117**, 1251 (1970).
[67]R. Gómez, A. Fernández-Vega, J. M. Feliu and A. Aldaz, J. Phys. Chem. **97**, 4769 (1993).
[68]N. M. Markovic, S. T. Sarraf, H. A. Gasteiger and P. N. Ross, J. Chem. Soc., Faraday Trans. **92**, 3719 (1996).
[69]T. J. Schmidt, P. N. Ross and N. M. Markovic, J. Electroanal. Chem. **524**, 252 (2002).
[70]B. E. Conway, J. Barber and S. Morin, Electrochim. Acta **44**, 1109 (1998).
[71]J. H. Barber and B. E. Conway, J. Electroanal. Chem. **461**, 80 (1999).
[72]B. E. Conway and B. V. Tilak, Electrochim. Acta **47**, 3571 (2002).
[73]N. Hoshi, Y. Asaumi, M. Nakamura, K. Mikita and R. Kajiwara, J. Phys. Chem. C **113** (39), 16843 (2009).
[74]R. Kajiwara, Y. Asaumi, M. Nakamura and N. Hoshi, J. Electroanal. Chem. **657**, 61 (2011).
[75]M. Nakamura, T. Kobayashi and N. Hoshi, Surf. Sci. **605**, 1462 (2011).
[76]J. Klein, A. K. Engstfeld, S. Brimaud and R. J. Behm, Phys. Chem. Chem. Phys. **22** (34), 19059 (2020).
[77]M. Zhou, S. J. Bao and A. J. Bard, J. Am. Chem. Soc. **141** (25), 10117 (2019).
[78]J. Greeley, T. F. Jaramillo, J. Bonde, I. B. Chorkendorff and J. K. Norskov, Nat. Mater. **5** (11), 909 (2006).
[79]P. Sabatier, Ber. Dtsch. Chem. Ges. **44**, 1984 (1911).
[80]D. Liu, X. Li, S. Chen, H. Yan, C. Wang, C. Wu, Y. A. Haleem, S. Duan, J. Lu, B. Ge, P. M. Ajayan, Y. Luo, J. Jiang and L. Song, Nat. Energy **4** (6), 512 (2019).
[81]M. T. Tang, X. Y. Liu, Y. F. Ji, J. K. Norskov and K. R. Chan, J. Phys. Chem. C **124** (51), 28083 (2020).
[82]T. L. Tan, L.-L. Wang, J. Zhang, D. D. Johnson and K. Bai, ACS Catal. **5** (4), 2376 (2015).
[83]L. Mei, X. Gao, Z. Gao, Q. Zhang, X. Yu, A. L. Rogach and Z. Zeng, Chem. Commun. **57** (23), 2879 (2021).
[84]D. V. Esposito, S. T. Hunt, A. L. Stottlemyer, K. D. Dobson, B. E. McCandless, R. W. Birkmire and J. G. Chen, Angew. Chem. Int. Ed. Engl. **49** (51), 9859 (2010).
[85]J. Yu, D. Wei, Z. Zheng, W. Yu, H. Shen, Y. Qu, S. Wen, Y. U. Kwon and Y. Zhao, J. Colloid Interface Sci. **566**, 505 (2020).

[86]Y. Tan, Y. Wei, K. Liang, L. Wang and S. Zhang, Int. J. Hydrogen Energy **46** (52), 26340 (2021).
[87]D. V. Esposito, S. T. Hunt, Y. C. Kimmel and J. G. G. Chen, J. Am. Chem. Soc. **134** (6), 3025 (2012).
[88]K. Nakada and I. Akira, in *Graphene Simulation* (InTech, 2011), pp. 3-21.
[89]M. Matsutsu, M. A. Petersen and E. van Steen, Phys. Chem. Chem. Phys. **18** (36), 25693 (2016).
[90]G. Ramos-Sanchez and P. B. Balbuena, Phys. Chem. Chem. Phys. **15** (28), 11950 (2013).
[91]W. B. Schneider, U. Benedikt and A. A. Auer, ChemPhysChem **14** (13), 2984 (2013).
[92]L. G. Verga, J. Aarons, M. Sarwar, D. Thompsett, A. E. Russell and C. K. Skylaris, Phys. Chem. Chem. Phys. **18** (48), 32713 (2016).
[93]C. Poidevin, P. Paciok, M. Heggen and A. A. Auer, J. Chem. Phys. **150** (4), 041705 (2019).
[94]M. Tavakkoli, N. Holmberg, R. Kronberg, H. Jiang, J. Sainio, E. I. Kauppinen, T. Kallio and K. Laasonen, ACS Catal. **7** (5), 3121 (2017).
[95]S. Ye, F. Luo, Q. Zhang, P. Zhang, T. Xu, Q. Wang, D. He, L. Guo, Y. Zhang, C. He, X. Ouyang, M. Gu, J. Liu and X. Sun, Energy Environ. Sci. **12** (3), 1000 (2019).
[96]X. P. Yin, H. J. Wang, S. F. Tang, X. L. Lu, M. Shu, R. Si and T. B. Lu, Angew. Chem. Int. Ed. **57** (30), 9382 (2018).
[97]J. Zhang, Y. Zhao, X. Guo, C. Chen, C.-L. Dong, R.-S. Liu, C.-P. Han, Y. Li, Y. Gogotsi and G. Wang, Nat. Catal. **1** (12), 985 (2018).
[98]S. Wang, X. Gao, X. Hang, X. Zhu, H. Han, W. Liao and W. Chen, J. Am. Chem. Soc. **138** (50), 16236 (2016).
[99]B. Hinnemann, P. G. Moses, J. Bonde, K. P. Jørgensen, J. H. Nielsen, S. Horch, I. Chorkendorff and J. K. Nørskov, J. Am. Chem. Soc. **127**, 5308 (2005).
[100]T. F. Jaramillo, K. P. Jørgensen, J. Bonde, J. H. Nielsen, S. Horch and I. Chorkendorff, Science **317**, 100 (2007).
[101]J. Kibsgaard, Z. Chen, B. N. Reinecke and T. F. Jaramillo, Nat. Mater. **11** (11), 963 (2012).
[102]H. Li, C. Tsai, A. L. Koh, L. Cai, A. W. Contryman, A. H. Fragapane, J. Zhao, H. S. Han, H. C. Manoharan, F. Abild-Pedersen, J. K. Norskov and X. Zheng, Nat. Mater. **15** (3), 364 (2016).
[103]Y. Yin, J. Han, Y. Zhang, X. Zhang, P. Xu, Q. Yuan, L. Samad, X. Wang, Y. Wang, Z. Zhang, P. Zhang, X. Cao, B. Song and S. Jin, J. Am. Chem. Soc. **138** (25), 7965 (2016).
[104]M. H. Miles and M. A. Thomason, J. Electrochem. Soc. **123**, 1459 (1976).
[105]R. Subbaraman, D. Tripkovic, D. Strmcnik, K.-C. Chang, M. Uchimura, A. P. Paulikas, V. Stamenkovic and N. M. Markovic, Science **334**, 1256 (2011).
[106]M. A. McArthur, L. Jorge, S. Coulombe and S. Omanovic, J. Power Sources **266**, 365 (2014).
[107]Y. F. Xu, M. R. Gao, Y. R. Zheng, J. Jiang and S. H. Yu, Angew. Chem. Int. Ed. Engl. **52** (33), 8546 (2013).
[108]X. Zou, X. Huang, A. Goswami, R. Silva, B. R. Sathe, E. Mikmekova and T. Asefa, Angew. Chem. Int. Ed. Engl. **126**, 4461 (2014).
[109]H. Fei, J. Dong, M. J. Arellano-Jimenez, G. Ye, N. Dong Kim, E. L. Samuel, Z. Peng, Z. Zhu, F. Qin, J. Bao, M. J. Yacaman, P. M. Ajayan, D. Chen and J. M. Tour, Nat. Commun. **6**, 8668 (2015).
[110]X. Wen, X. Yang, M. Li, L. Bai and J. Guan, Electrochim. Acta **296**, 830 (2019).